Journal of Biomechanics 90 (2019) 50–57

Contents lists available at ScienceDirect

Journal of Biomechanics

journal homepage: www.elsevier.com/locate/jbiomech
www.JBiomech.com

Role of diastolic vortices in flow and energy dynamics during systolic ejection

Vivek Vasudevan [a], Adriel Jia Jun Low [a], Sarayu Parimal Annamalai [b], Smita Sampath [b], Chih-Liang Chin [b], Asad Abu Bakar Ali [b], Choon Hwai Yap [a,*]

[a] Department of Biomedical Engineering, National University of Singapore, Singapore
[b] Pacific Translational Biomarkers, MRL, MSD, Singapore

ARTICLE INFO

Article history:
Accepted 16 April 2019

Keywords:
Left ventricle
Computational fluid dynamics
Intra-cardiac fluid mechanics
Diastolic vortices
Apical washout

ABSTRACT

MRI-based computational fluid dynamics simulations were performed in the left ventricles of two adult porcine subjects with varying physiological states (before and after an induced infarction). The hypothesis that diastolic vortices store kinetic energy and assist systolic ejection was tested, by performing systolic simulations in the presence and absence of diastolic vortices. The latter was achieved by reinitializing the entire velocity field to be zero at the beginning of systole. A rudimentary prescribed motion model of a mitral valve was included in the simulations to direct the incoming mitral jet towards the apex. Results showed that the presence or absence of diastolic vortex rings had insignificant impact on the energy expended by walls of the left ventricles for systolic ejection for both the porcine subjects, under all physiological conditions. Although substantial kinetic energy was stored in diastolic vortices by end diastole, it provided no appreciable savings during systolic ejection, and most likely continued to complete dissipation during systole. The role of diastolic vortices in apical washout was investigated by studying the cumulative mass fraction of passive dye that was ejected during systole in the presence and absence of vortices. Results indicated that the diastolic vortices play a crucial role in ensuring efficient washout of apical blood during systolic ejection.

1. Introduction

Left ventricular (LV) fluid mechanics during diastole is characterized by vortex rings brought about by mitral inflow. The characteristics of these vortex rings have been studied in detail with idealized (Cheng et al., 2005; Domenichini et al., 2005) and physiologically accurate (Mihalef et al., 2011; Seo et al., 2014; Vedula et al., 2016) LV models, via clinical MRI (Elbaz et al., 2014) and ultrasound imaging (Pedrizzetti et al., 2014). It was previously proposed that vortices formed in healthy LV chambers reduce energy expenditure during blood pumping and transit through the heart (Kilner et al., 2000). In particular, it was proposed that the diastolic vortex rings can store kinetic energy of blood flow, which can then be brought over into the subsequent systole to reduce energy expenditure needed for ejection. However, there were reports corroborating (Pedrizzetti and Domenichini, 2005) and disputing (Watanabe et al., 2004) this theory, and a definitive conclusion has yet to be reached.

Understanding and quantification of the fluid and energy dynamics of a healthy heart is important, so as to establish a firmer understanding of the heart under baseline conditions, which can then help in analyzing diseased hearts. This is also important in diseases associated with heart failures, wherein there is difficulty generating sufficient energy for circulation. In terms of quantifying energy dynamics of flow, image-based computational fluid dynamics (CFD) remains a very good tool, as it is fully 4D, has a high resolution and is able to capture fluid shear gradients effectively (Lai et al., 2015; Le and Sotiropoulos, 2012; Schenkel et al., 2009). Multiple authors have utilized CFD simulations to assess fluid and energy dynamics in the heart (Ho et al., 2017; Seo et al., 2014; Vedula et al., 2016; Wiputra et al., 2017).

In this study, we performed MRI-based CFD simulations on LV of two adult porcine subjects with varying physiological states (before and after an induced infarction). We tested the hypothesis that diastolic vortices store kinetic energy and assist systolic ejection by performing systolic simulations in the presence and absence of diastolic vortices. We also quantified the role of diastolic vortices in flushing out apical blood from the left ventricle during a cardiac cycle. In modelling the LV, it is important to

* Corresponding author.
E-mail address: bieyapc@nus.edu.sg (C.H. Yap).

https://doi.org/10.1016/j.jbiomech.2019.04.026
0021-9290/

include mitral valves, as they are known to assist ventricular filling (Charonko et al., 2013) and enhance apical washout (Seo et al. 2014; Vedula et al, 2016). A simplified mitral valve model was therefore included in the current study. A minor secondary objective was to examine how the inclusion of mitral valve in the simulations affected flow and energy dynamics.

2. Methodology

2.1. Animal model, MRI acquisition and LV reconstruction

Myocardial infarction (MI) was induced in two porcine subjects through permanent ligation of left circumflex coronary artery (LCx). Animals were stabilized at a baseline heart rate of about 70 bpm. All intervention and imaging experiments were reviewed and approved by Merck & Co., Inc. (WestPoint, PA, USA), and the Institutional Animal Care and Use Committee (IACUC) at The National University of Singapore.

MR imaging scans were performed on both porcine subjects (#1 and #2) at 3 time points, pre-LCx (baseline, "W_0"), one week (acute, "W_1") and four weeks (chronic, "W_4") post-LCx. CINE images along the short-axis were captured in the basal to apical direction (at a through-plane distance of 10 mm) with 25 images per cardiac cycle in each scan. The myocardial twisting motion was quantified via SPAMM tagging (Axel and Dougherty, 1989) and Harmonic Phase (HARP) (Osman and Prince, 2000) analyses.

Reconstruction of LV model at each time point of the cardiac cycle was performed in Vascular Modelling Toolkit (VMTK, www.vmtk.org) via a level-set segmentation algorithm. Geomagic Studio® (Geomagic Inc., Morrisville, NC, USA) was used to smooth the segmented 3D LV surfaces, and to calculate LV volume and centroid at each time point.

2.2. Mathematical modelling of LV wall motion

Mathematical modelling of LV wall motion was performed using previously established methods (Vasudevan et al., 2017), wherein greater details of methods and limitations are discussed. Briefly, a spherical coordinate system was employed from the centroid, and the motion of each LV wall node was described as a combination of motion in the radial direction, and motion in the azimuthal direction corresponding to LV twist. All parts of the LV wall were assumed to move in phase. The model did not account for aphasic movement of infarcted tissue, and therefore effects of infarction were limited to changes in radial motions only. The amplitude of angular twist was assumed to increase linearly from LV base to apex. The characteristic waveforms for radial and twist motion were assumed to be the same, as both were results of the same myocardial contractions, and were obtained from velocity measurements at the LV inlet and outlet using principles of conservation of mass.

2.3. Mathematical modelling of mitral valve (MV) motion

MV geometry was based on detailed anatomical measurements from a database of 10 adult porcine specimens (Kunzelman et al., 1994). The leaflets were idealized to be straight and rigid with lengths varying from 20 mm (at tip of anterior leaflet, AL) and 12 mm (at tip of posterior leaflet, PL), to 7 mm (at tips of anterolateral, AL-C, and posteromedial, PM-C, commissures). The digitally reconstructed MV was then inserted into the reconstructed LV model (Fig. S1).

Motion of MV leaflets was modelled using a prescribed kinematics model. The opening angles (angles between MV leaflets and mitral orifice plane) were measured at different cardiac phases in the 3-chamber view. Temporal resolution of the scans was insufficient to accurately capture the rapid opening and closing of the MV leaflets resulting in some errors in leaflet position during the rapid opening/closing phases. A 7th order Fourier series was fitted to the measured average opening angles to describe leaflet dynamics. Coaptation was avoided by gradually shortening the medial-lateral lengths of the leaflets whenever the gap between leaflet tips was below a user-defined threshold.

2.4. Computational fluid dynamics (CFD) simulation

Dynamic mesh CFD simulations were performed in ANSYS Workbench Suite (ANSYS, Inc., Canonsburg, PA, USA) using previously established methods (Lai et al., 2015; Wiputra et al., 2016). User-defined functions (UDFs) were employed to specify motions of LV wall and MV leaflets. Simulations were performed for four cardiac cycles to remove initial condition artefacts, and results from the fourth cardiac cycle were used for analysis. Convergence criteria was set to be less than 10^{-4} for all scaled residuals. A power-law model for non-Newtonian fluids was used for the apparent viscosity of porcine blood (Rosentrater and Flores, 1997), while the density was set at 1021.6 kg/m^3.

Boundary conditions chosen were such that during diastole, mitral opening was specified as zero pressure inlet and LVOT was specified as a wall. Conversely, during systole, mitral opening was specified as a wall, while LVOT was a zero pressure outlet. Pressure elsewhere in the ventricle was expressed as a differential from these reference pressures, and were used to calculate LV work.

2.5. Effects of diastolic vortices on systolic ejection

To remove the influence of diastolic vortices on systolic ejection, velocity and pressure fields were reinitialised to zero at the beginning of systole. Simulations were conducted for only the systolic phase in the absence of diastolic vortices, and results were compared to simulations where diastolic vortices were present. Energy dynamics parameters, quantified according to previous methods (Vasudevan et al., 2017), are briefly explained here. Total systolic energy loss ($EL_{syst.}$) was calculated via laws of conservation of energy as follows: contraction work done by LV during systole ($W_{syst.}$) provided kinetic energy (KE) to blood exiting the LV (KE_{out}) and also increased KE of blood within the LV over systole ($\Delta KE_{syst.}$).

$$EL_{syst.} = W_{syst.} - KE_{out} - \Delta KE_{syst.} \tag{1}$$

$$\widehat{EL}_{syst.} = \frac{EL_{syst.}}{SV} \tag{2}$$

Specific systolic energy loss ($\widehat{EL}_{syst.}$), obtained by normalizing $EL_{syst.}$ with stroke volume (SV), reflected the energy loss per unit volume of blood pumped by the heart. These energy terms reflected only the work done to overcome viscous energy losses experienced by the flow, and did not include work done to overcome afterload. Terms in Eqs. (1) and (2) were defined as:

$$W_{syst.} = \int_{systole}\int_{LVWall} P\left(\vec{v}.\hat{n}\right)dAdt \tag{3}$$

$$KE_{out} = \int_{t_{syst.}}\int_{outlet} \frac{1}{2}\rho v^2\left(\vec{v}.\hat{n}\right)dAdt \tag{4}$$

$$\Delta KE_{syst.} = \left(\int_{Vol_{LV}} \frac{1}{2}\rho v^2 dV\right)\Big|_{t_{syst}} \tag{5}$$

where ρ was density, $\vec{v}$ was velocity vector, $\hat{n}$ was unit normal to surface boundary, P was fluid pressure, Vol_{LV} was LV volume, and $t_{syst.}$ was systolic duration. Systolic time- and volume-averaged KE density ($\overline{KE}_{syst.}$) and systolic time- and surface-averaged wall shear stress ($\overline{WSS}_{syst.}$) were calculated as:

$$\overline{KE}_{syst.} = \frac{1}{t_{syst.}} \int_{t_{syst.}} \left[\frac{1}{Vol_{LV}} \int_{Vol_{LV}} \frac{1}{2} \rho v^2 dV \right] dt \tag{6}$$

$$\overline{WSS}_{syst.} = \frac{1}{t_{syst.}} \int_{t_{syst.}} \left[\frac{1}{Area_{LV}} \int_{Area_{LV}} \mu \frac{\partial \vec{v}}{\partial \hat{n}} dA \right] dt \tag{7}$$

where $Area_{LV}$ was LV surface area. KE in the LV chamber at end-diastole (KE_{EDV}) (Eq. (8)) was calculated to quantify the diastolic KE that was passed on to the subsequent systolic phase. Average KE flux exiting the LVOT during systole ($KE_{flux,syst.}$) (Eq. (9)) and maximum velocity at LVOT ($Max.v_{LVOT}$) were calculated for cases with and without diastolic vortices, to verify that the results were not biased to either category.

$$\mathrm{KE}_{EDV} = \left(\int_{Vol_{LV}} \frac{1}{2} \rho v^2 dV \right) \Big|_{t=t_D} \tag{8}$$

$$KE_{flux,syst.} = \frac{1}{t_s} \int_{t_s} \left[\frac{1}{A_{LVOT}} \int_{A_{LVOT}} \frac{1}{2} \rho v^2 \left(\vec{v}.\hat{n} \right) dA \right] dt \tag{9}$$

2.6. Effects of diastolic vortices on apical washout

Efficient washout of apical blood is essential to prevent flow stasis. Transport of a passive dye was modelled to quantify washout efficiency. The passive dye was initialized in the apical region (defined as 10 mm from LV apex) at end-diastole (during the 4th cardiac cycle). Diffusivity coefficient of dye (in blood) was set to be very low (10^{-9} m^2/s). Washout effectiveness was gauged by the mass fraction of dyed blood remaining in the apical region and the fraction ejected at the end of one systolic beat.

3. Results

3.1. Physiological details of segmented porcine hearts

Table 1 lists the physiological parameters of the simulated porcine hearts, and demonstrates the changes due to induced infarction. Generally, heart rate increased, ejection fraction decreased, and ventricular volume increased acutely and recovered slightly at four weeks post-infarction. Readers are directed to our earlier work for a detailed analysis of the effects of these changes on LV fluid and energy dynamics (Vasudevan et al., 2017). From MRI scans, infarctions were found in the inferior and lateral regions of the LV. Generally, positive remodelling were observed from week 1 to 4, with a reduction in percentage infarct from 20% to 11% for subject #1, and from 22% to 15% for subject #2.

3.2. Mesh convergence study

Grid dependency analysis was performed to arrive at an optimum grid size that was computationally feasible, and yet captured the essential features of LV fluid and energy dynamics. Four different grids were generated: 300 K, 700 K, 1.9 M and 2.9 M cells. Fig. 1a and b shows the temporal evolution of work done (W_{cycle}) and energy loss (ΔE_{cycle}) during a cardiac cycle for cases with different mesh densities. Comparing between 1.9 M and 2.9 M, cumulative LV work done changed by 0.5% and total energy loss changed by less than 3% (Fig. 1a and b). Further, vortex structures visualized

Table 1
Physiological parameters of the MR scanned hearts.

	Subject #1 (6 month female)			Subject #2 (4 month female)		
	#1W_0	#1W_1	#1W_4	#2W_0	#2W_1	#2W_4
Heart rate (bpm)	63	93	95	66	94	90
$t_{Diastole} : t_{Systole}$	61:39	51:49	48:52	46:54	55:45	51:49
EDV (ml)	92	136	95	95	112	107
SV (ml)	48	63	34	50	55	48
Ejection fraction (%)	52	46	36	53	50	45
Cardiac output (L/min)	3.0	5.9	3.3	3.3	5.2	4.3

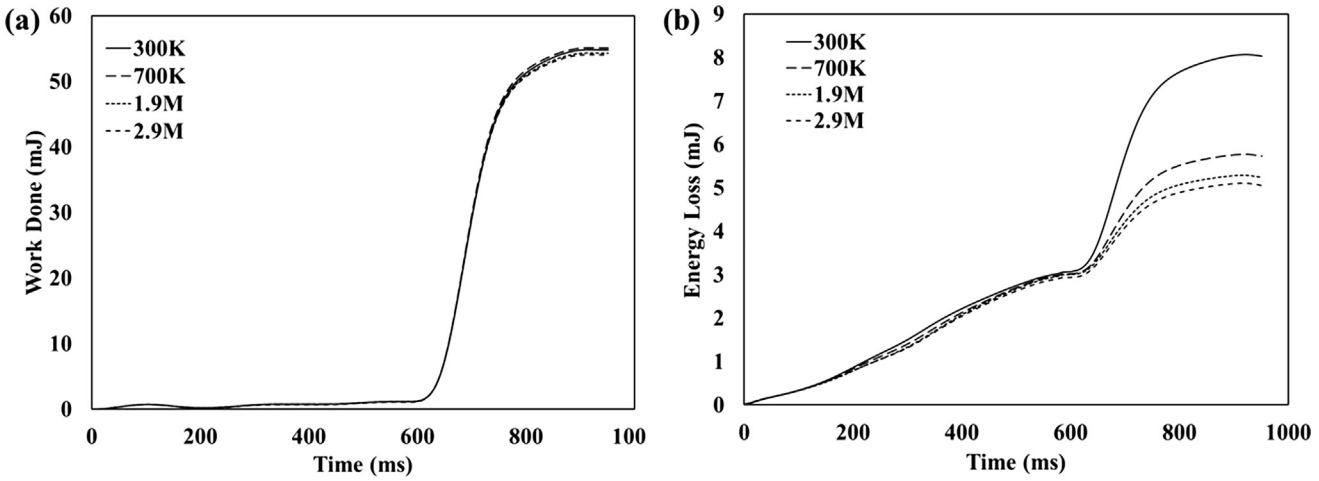

Fig. 1. Grid sensitivity analysis for 4 different grids (300 K, 700 K, 1.9 M, 2.9 M cells). Evolution of (a) Work done and (b) Energy Loss during a cardiac cycle for 4 grids.

Table 2
Total energy loss over the cardiac cycle normalized by stroke volume ($\hat{E}$), time-averaged diastolic kinetic energy density ($\overline{KE}_{diast.}$), and time- and surface-averaged diastolic wall shear stresses ($\overline{WSS}_{diast.}$) for simulated LV chambers.

	With/without mitral valve	$\hat{E}$ (mJ/litre)	$\overline{KE}_{diast.}$ (mJ/litre)	$\overline{WSS}_{diast.}$ (Pa)
#1W_0	Without	49	6.6	0.78
	With	111	16.9	1.18
#1W_1	Without	170	29.2	1.58
	With	502	71.1	2.50
#1W_4	Without	91	14.4	1.07
	With	194	27.8	1.20
#2W_0	Without	103	16.8	1.15
	With	291	37.8	1.47
#2W_1	Without	159	23.0	1.19
	With	375	48.9	1.73
#2W_4	Without	174	36.0	1.70
	With	619	81.7	2.49

at peak E-wave were sufficiently similar between the two meshes. We therefore adopted a criteria that mesh size should be a minimum of 1.9 M elements.

3.3. Effects of mitral valves on flow and energy dynamics

Flow changes observed due to the inclusion of the mitral valve were formation of vortex rings at the tip of the valve leaflets instead of at the mitral annulus, and narrowing of the inflow jet (Fig. S3). The penetration depth of the incoming jet increased, and the intensity of vortex dynamics and chaotic flow was enhanced (higher diastolic KE density, Table 2). Consequently, energy losses were higher due to higher wall shear stresses (WSS), and higher viscous dissipation between rapidly moving fluid layers in the bulk flow.

However, it was interesting that addition of the mitral valves did not alter the sequence of which heart had higher or lower energy dynamics indices (Fig. S4). In other words, if all simulation cases were ranked in their specific energy loss magnitude or diastolic KE density magnitude, the ranks for all simulation cases would be retained irrespective of the presence or absence of mitral valves. Hence, simulations without mitral valves might be sufficient to investigate trends in changes in LV energy dynamics due to myocardial infarction.

3.4. Role of diastolic vortices on systolic energy dynamics

Fig. 2 shows vorticity iso-surfaces calculated based on λ_2 criterion (Jeong and Hussain, 1995) and WSS distribution on LV wall for subject #1. These data are also available as online supplementary videos. Diastolic vortex rings corresponding to E- and A-waves were observed, together with complex secondary vorticity structures caused by their interactions with LV wall. Further, in cases where diastolic vortices were removed, very few vorticity structures developed during systole.

Table 3 lists the various energy indices during systolic ejection for simulations in presence and absence of diastolic vortices. There were insignificant differences in outflowing KE ($KE_{flux.syst.}$) and maximum outflowing velocity ($Max.v_{LVOT}$) between cases with and without diastolic vortices. Neither category was thus biased to do additional ejection work. Although hearts with diastolic vortices had more KE at the beginning of systole (higher KE_{EDV}) (Table 3), they suffered more energy losses during systole (higher $\widehat{EL}_{Syst.}$), most likely due to higher fluid stresses and wall shear stresses (higher $\overline{WSS}_{syst.}$) caused by the more dynamic vorticity structures. Systolic work needed for ejection ($W_{syst.}$) showed negligible changes with or without diastolic vortices, suggesting that KE stored in these diastolic vortices dissipated away during systole instead of assisting outflow. Further, systolic work was about two orders of magnitude higher than systolic energy losses and KE densities. As such, even if the stored KE helped with systolic ejection, their contribution would be insignificantly small. In some cases, energy needed for ejection increased, presumably due to an obstruction to systolic ejection caused by the presence of these vortices.

Fig. 3 shows the evolution of energy indices during systolic ejection for two simulation cases, one with low amount of diastolic KE brought over into systole (#1W_0) and another with a larger amount (#1W_1). KE carried by diastolic vortices (KE_{EDV}) contributed significantly to the overall KE in the LV during systole, especially for #1W_1 (Fig. 4b). However, systolic energy losses were also higher due to increased shear interactions of the diastolic vortices, (higher $\overline{WSS}_{syst.}$ for cases with diastolic vortices in Table 3) and a more dynamic vorticity field in the bulk fluid. These resulted in insignificant differences in work done by the LV wall for systolic ejection, both in the presence and absence of diastolic vortices (Fig. 3). These same observations applied to all the other hearts simulated in this work, irrespective of whether the end-diastolic vorticity dynamics consisted of clear and distinct vortex rings or distributed secondary vortices. All these results implied that the remnant diastolic KE brought over into systole (KE_{EDV}) merely dissipated away over the course of systole, without aiding ejection efforts.

3.5. Role of diastolic vortices on washout of apical blood

Fig. 4a shows the volume fraction of dye and in-plane velocity vectors plotted on a 2D plane that cuts through the middle of the LVOT and mitral opening for subject #1. The diastolic vortices are responsible for washing out blood from the apical region, and thus lowering the possibility of apical blood stasis. Cumulative mass fraction of the dyed blood ejected during the systolic phase for all hearts was 0.30 ± 0.23, and varied from 0.00 to 0.65 (Table 4), depending on their cardiac outputs. Fig. 4b shows a bar plot of the mass fraction of dyed blood remaining in the apical region for all hearts at the end of systolic ejection. In the absence of vortices, the mass fraction of dyed blood remaining in the apical region remained close to unity, and consequently, the fraction of dye ejected was zero, for all hearts. This corroborated with observations by other researchers (Seo et al. 2014; Vedula et al. 2016) that the diastolic vortices played a key role in an efficient washout of LV blood. The effect of myocardial infarction on efficiency of apical blood washout was inconclusive, and depended on the flow dynamics of respective LVs.

4. Discussion

The current simulations were modified from our previous study (Vasudevan et al., 2017), in that a rudimentary mitral valve model

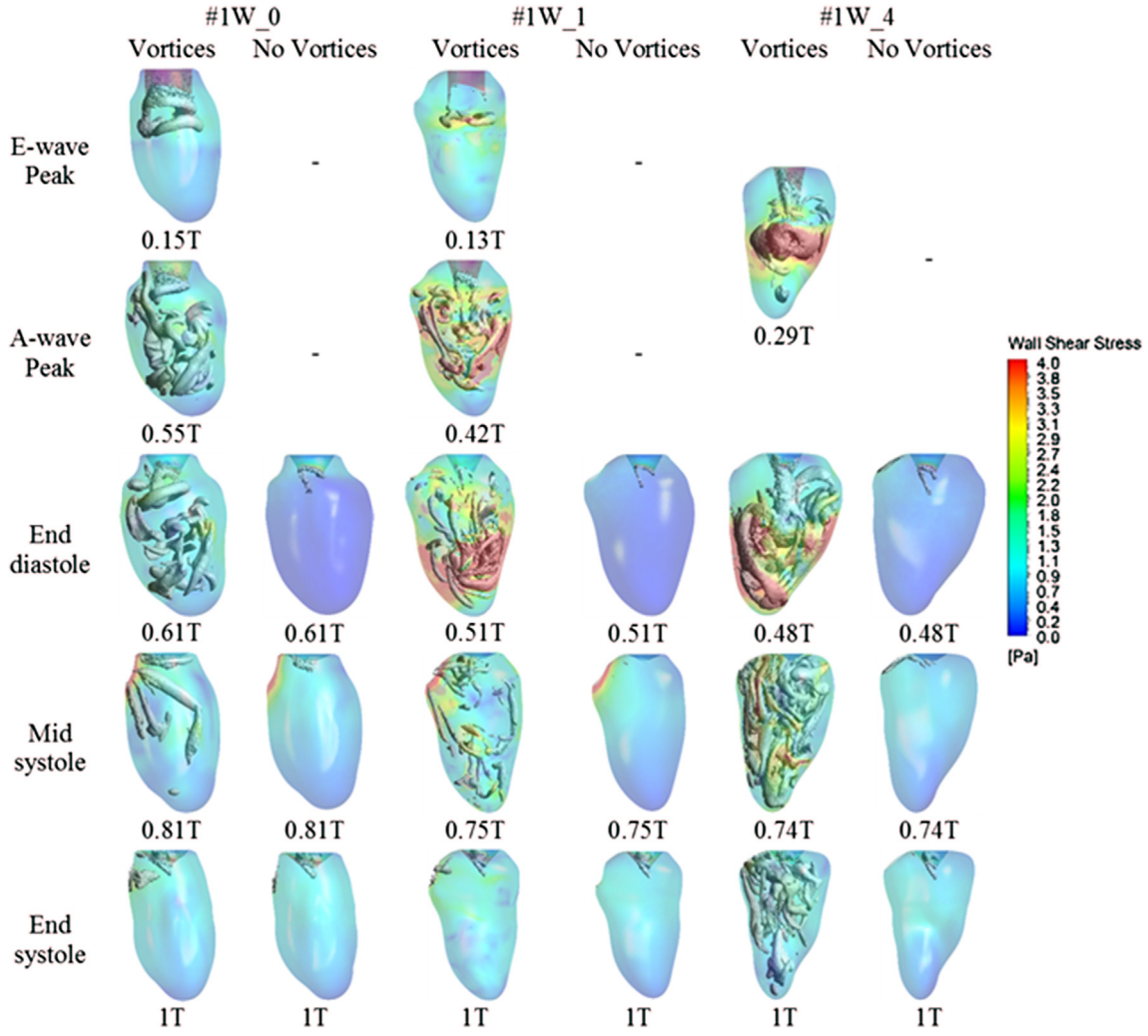

Fig. 2. Isosurface of vortex rings formed in the reconstructed left ventricles for subject #1 using λ_2 criterion ($-400\ s^{-2}$) at various time points in the cardiac cycle (additional results are presented in the form of videos in supplementary material).

Table 3
Effect of diastolic vortices on energy dynamics of left ventricles during systolic ejection, for cases with and without diastolic vortices. $\widehat{EL}_{Syst.}$ – energy loss per stroke volume, $\bar{KE}_{syst.}$ – systolic time- and volume-averaged KE density, KE_{EDV} – KE at end diastole, $W_{syst.}$ – total systolic contraction work done by the LV, $KE_{flux.syst.}$ – average systolic KE flux through the LVOT, $Max.v_{LVOT}$ – maximum velocity at the LVOT, $WSS_{syst.}$ – time- and surface-averaged systolic wall shear stress.

		$\widehat{EL}_{Syst.}$ (mJ/litre)	$\bar{KE}_{syst.}$ (mJ/litre)	KE_{EDV} (mJ)	$W_{syst.}$ (J/litre)	$KE_{flux.syst.}$ (mW/mm^2)	$Max.v_{LVOT}$ (m/s)	$\bar{WSS}_{syst.}$ (Pa)
#1W_0	Vortices	48	13.4	0.90	1.12	0.93	1.94	1.06
	No vortices	34	9.4	0.00	1.12	0.92	1.95	0.90
#1W_1	Vortices	222	43.6	13.82	1.69	2.02	2.12	2.24
	No vortices	37	13.0	0.00	1.69	1.98	2.12	1.14
#1W_4	Vortices	113	26.5	3.42	0.99	0.63	1.77	1.67
	No vortices	27	7.1	0.00	0.97	0.62	1.75	0.78
#2W_0	Vortices	121	21.1	5.47	0.73	0.47	1.77	1.57
	No vortices	20	5.9	0.00	0.73	0.46	1.77	0.72
#2W_1	Vortices	235	54.4	12.55	3.39	4.01	3.65	2.72
	No vortices	58	19.0	0.00	3.47	4.05	3.67	1.32
#2W_4	Vortices	160	33.1	7.20	2.29	2.93	2.83	2.18
	No vortices	27	9.7	0.00	2.27	2.87	2.81	0.93

with prescribed motion was also incorporated, as the valve is known to have significant influence on vortex dynamics. Inclusion of the mitral valve in the simulations resulted in increased density of vortex structures, more chaotic flow and higher KE, deeper penetration of diastolic inflow towards the apex, higher average wall shear stresses, and higher energy losses (Fig. S3, and Table 2). These results agreed with previous studies (Seo et al. 2014). However, interestingly, the inclusion of mitral valve did not rearrange the sequence of which heart condition had greater or lesser energy dynamics due to infarction (Fig. S4). This suggested that if the goal of the simulation is to compare energy dynamics between different scenarios and not to visualize flow patterns, simulations can be

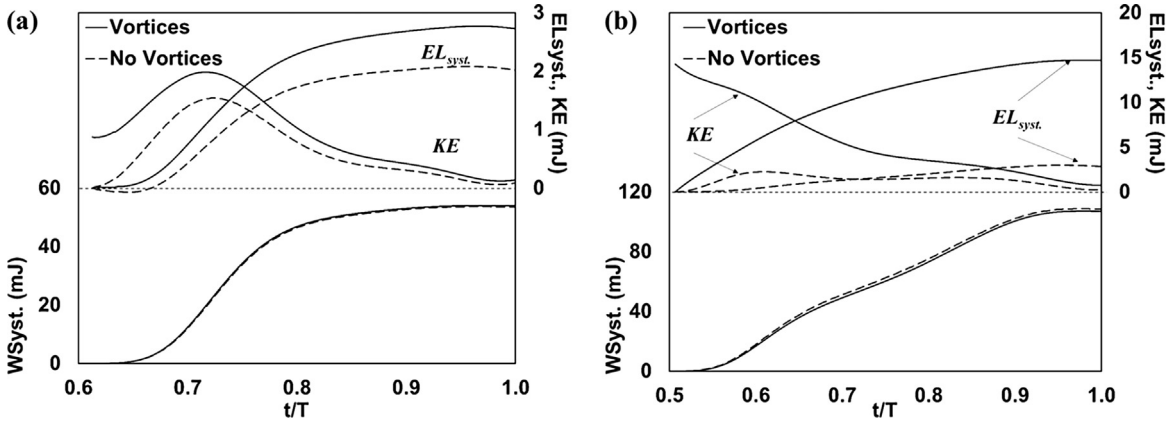

Fig. 3. Evolution of systolic work done ($W_{syst.}$), systolic energy loss ($EL_{syst.}$) and bulk systolic kinetic energy (KE) for a) #1W_0 and b) #1W_1.

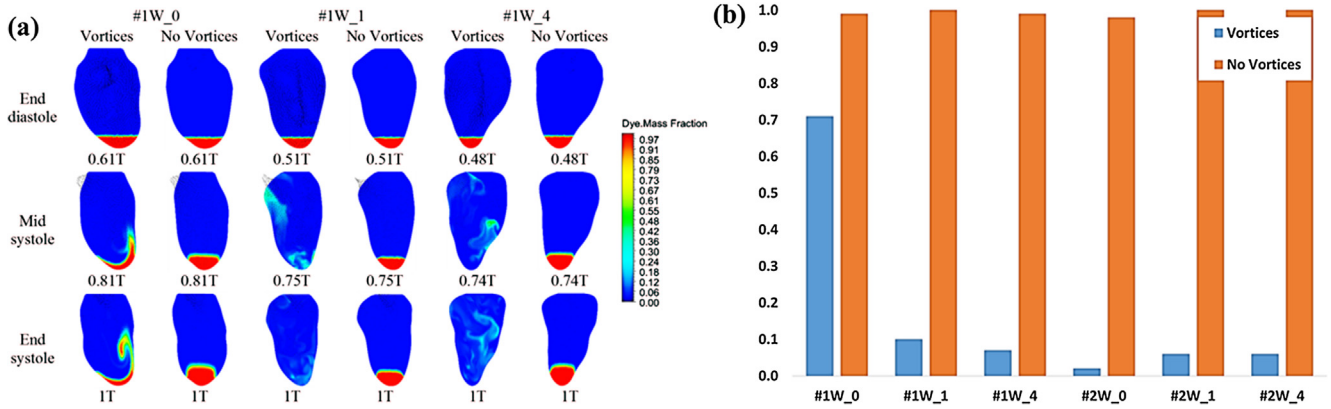

Fig. 4. (a) Contour maps of passive dye volume fraction and in-plane velocity vectors in the middle of the reconstructed porcine left ventricles for #1 (additional results are presented in the form of videos in supplementary material) (b) Mass fraction of dyed blood remaining in apical region at the end of systolic ejection.

Table 4
Fraction of dye ejected (by mass) and mass fraction of dye remaining in the apical region at the end of systole for all LVs in the presence and absence of diastolic vortices.

		Fraction of dye ejected during systole (by mass)	Mass fraction of dye in apical region at end of systole
#1W_0	Vortices	0.00	0.71
	No vortices	0.00	0.99
#1W_1	Vortices	0.65	0.10
	No vortices	0.00	1.00
#1W_4	Vortices	0.28	0.07
	No vortices	0.00	0.99
#2W_0	Vortices	0.46	0.02
	No vortices	0.0	0.98
#2W_1	Vortices	0.26	0.06
	No vortices	0.00	1.00
#2W_4	Vortices	0.14	0.06
	No vortices	0.00	1.00

performed without the mitral valve to reduce computational time. In our earlier study, we described a non-dimensional number (ratio of Reynolds to Strouhal number) that could represent the efficiency of flow in the LV (Vasudevan et al., 2017). This parameter was found to be valid even in the presence of mitral valves, as seen in Fig. S5.

The main finding of our study was that KE stored in the diastolic vortices provided no appreciable energy savings for systolic ejection (Table 3). Hearts under different physiological conditions (pre- and post-infarct, different heart rates, stroke volume and ventricular sizes) were investigated, and the same conclusion was reached. There has been much conjecture in the scientific community regarding the energy-saving capacity of diastolic vortex rings. The asymmetric nature of flow in the normal LV and the consequent LV vortices were thought to reduce energy dissipation and facilitate an efficient ejection of blood by redirecting blood velocities towards the outflow tract (Kilner et al., 2000), and investigators proposed that the vortices played the role of storing KE for use during systole (Hong et al., 2008; Khalafvand et al., 2015). A particular study (Pedrizzetti and Domenichini, 2005) found that a slightly asymmetric position of the mitral valve, as opposed to a symmetric central position or an extremely asymmetric position, had minimum energy losses, supporting the above theory.

However, Watanabe et al. (2004) found that work done by LV wall did not change between cases with a physiological and non-physiological flow pattern. Likewise, in another study (Seo et al., 2014), pumping efficiency calculations for cases with varying E/A ratios and varying mitral valve locations showed that end-diastolic flow patterns could bring about approximately 200 Pa of pressure changes, which was insignificant when compared to the afterload of the heart.

In the current study, this issue was re-examined by simulating blood stasis via the removal of the end-diastolic vortices and comparing the resulting systolic simulations to cases where diastolic vortices were present. Results corroborated with Watanabe et al.'s (2004) and Seo et al.'s (2014) studies as we observed that the vortices did not impact systolic ejection energetics. The KE of

end-diastolic vortices continued to complete dissipation during systole, and despite timing overlap with systolic outflow, did not lead to a reduction in work done needed for outflow. Diastolic vortex rings and secondary vortex structures are highly 3D in nature, and we suggest that while certain 2D cut-plane diagrams might indicate a redirection alignment towards the outflow tract, care should be taken that little of the flow may actually align towards the outflow tract in 3D. We further opine that Pedrizzetti and Domenichini's (2005) results on how an asymmetric inflow was more energy efficient, were a reflection that the asymmetric inflow was an energy efficient way of ventricular filling (the energy savings could be realized over both diastole and the subsequent systole, since vortex dissipations would continue into systole), rather than a demonstration of the vortices having any contribution towards systolic ejection. Several subsequent authors (Belohlavek, 2012; Martínez-Legazpi et al., 2014) have discussed and supported the notion reported by Pedrizzetti and Domenichini that diastolic vortices are a means to increase LV filling efficiency.

Passive dye ejection simulations showed that diastolic vortices played a key role in fluid exchange at the LV apex, resulting in efficient LV fluid washout. In the absence of diastolic vortices, little passive dye at the apical region was ejected, indicating a likelihood of thrombus formation. Risk of LV thrombus formation has been reported to be high in acute myocardial infarction (AMI) cases (Delewi et al., 2012). In our simulations, efficiency of apical blood washout depended on the effect of myocardial infarction on fluid dynamic and cardiac output of the LVs. It was generally observed that at acute and chronic time-points (W_1 and W_4), less than 10% of apical blood remained in the apical region at the end of one systolic ejection (Table 4), suggesting that the infarction cases in our animal study had a relatively high washout efficiency.

5. Limitations

In the current study, simulations were limited to two porcine subjects, which might be insufficient to fully account for biological variability. The mitral valve motion was modelled not with Fluid-Structure Interaction (FSI) simulations, but with a prescribed leaflet kinematics model. This most likely caused errors, especially with regards to finer details such as flow near the leaflets or during rapidly moving phases. However, the valve model employed could still shape the inflow stream and influence diastolic vortices in its open phases, which was the objective of modelling the valve.

The CFD model did not include realistic absolute pressures, and only modelled and spatial pressure gradients. However, afterload could be superimposed onto the simulated CFD pressure fields to obtain realistic absolute LV pressures.

Although the diastole:systole duration ratio in subject #2 was unusually low, no detectable signs of disease or abnormality was noted in the subject before inducing infarction, and as such may be an outlying case due to biological variability.

Finally, our approach of simulating blood stasis for the "no diastolic vortex" case is only one out of many possible approaches to test the role of diastolic vortices in assisting systolic ejection, and cannot be construed as representative of all possible scenarios of removing physiologic diastolic vortices.

6. Conclusions

MR image-based CFD simulations of blood flow were conducted in the left ventricles of two adult porcine subjects at various physiological states. The role of diastolic vortices in energy dynamics of systolic ejection was tested, but results showed that they did not help reduce the work done necessary for systolic ejection. Diastolic vortices, however, were crucial in flushing blood from the apical regions during each cardiac cycle, and thereby reduced the possibility of thrombus formation at the LV apex. These observations were consistent for all simulations performed in this study, before and after myocardial infarction, and across various heart rates, stroke volumes, and ventricular sizes.

Acknowledgement

This study was funded by the Singapore Millennium Foundation Grant entitled "Minimally-invasive, Thoracoscopic-ally Implantable Cardiac Assist Device for Palliative Care of the Elderly with Failing Hearts" (PI: Yap, awarded in 2014). The authors thank Yvonne Tay and Elaine Manigbas for their assistance with MR data acquisition.

Conflict of interest statement

All authors have no conflict of interest to declare.

Appendix A. Supplementary data

Supplementary data to this article can be found online at https://doi.org/10.1016/j.jbiomech.2019.04.026.

References

Axel, L., Dougherty, L., 1989. MR imaging of motion with spatial modulation of magnetization. Radiology 171, 841–845.
Belohlavek, M., 2012. Vortex Formation Time: An Emerging Echocardiographic Index of Left Ventricular Filling Efficiency? Oxford University Press.
Charonko, J.J., Kumar, R., Stewart, K., Little, W.C., Vlachos, P.P., 2013. Vortices formed on the mitral valve tips aid normal left ventricular filling. Ann. Biomed. Eng. 41, 1049–1061.
Cheng, Y., Oertel, H., Schenkel, T., 2005. Fluid-structure coupled CFD simulation of the left ventricular flow during filling phase. Ann. Biomed. Eng. 33, 567–576.
Delewi, R., Zijlstra, F., Piek, J.J., 2012. Left ventricular thrombus formation after acute myocardial infarction. Heart 98, 1743–1749.
Domenichini, F., Pedrizzetti, G., Baccani, B., 2005. Three-dimensional filling flow into a model left ventricle. J. Fluid Mech. 539, 179–198.
Elbaz, M.S., Calkoen, E.E., Westenberg, J.J., Lelieveldt, B.P., Roest, A.A., van der Geest, R.J., 2014. Vortex flow during early and late left ventricular filling in normal subjects: quantitative characterization using retrospectively-gated 4D flow cardiovascular magnetic resonance and three-dimensional vortex core analysis. J. Cardiovasc. Magn. Reson. 16, 78.
Ho, S., Tan, G.X.Y., Foo, T.J., Phan-Thien, N., Yap, C.H., 2017. Organ dynamics and fluid dynamics of the HH25 chick embryonic cardiac ventricle as revealed by a novel 4D high-frequency ultrasound imaging technique and computational flow simulations. Ann. Biomed. Eng. 45, 2309–2323.
Hong, G.-R., Pedrizzetti, G., Tonti, G., Li, P., Wei, Z., Kim, J.K., Baweja, A., Liu, S., Chung, N., Houle, H., 2008. Characterization and quantification of vortex flow in the human left ventricle by contrast echocardiography using vector particle image velocimetry. JACC: Cardiovasc. Imag. 1, 705–717.
Jeong, J., Hussain, F., 1995. On the identification of a vortex. J. Fluid Mech. 285, 69–94.
Khalafvand, S.S., Hung, T.-K., Ng, E.Y.-K., Zhong, L., 2015. Kinematic, dynamic, and energy characteristics of diastolic flow in the left ventricle. Computational and mathematical methods in medicine 2015.
Kilner, P.J., Yang, G.-Z., Wilkes, A.J., Mohiaddin, R.H., Firmin, D.N., Yacoub, M.H., 2000. Asymmetric redirection of flow through the heart. Nature 404, 759.
Kunzelman, K.S., Cochran, R.P., Verrier, E.D., Eberhart, R.C., 1994. Anatomic basis for mitral valve modelling. J. Heart Valve Dis. 3, 491–496.
Lai, C.Q., Lim, G.L., Jamil, M., Mattar, C.N., Biswas, A., Yap, C.H., 2015. Fluid mechanics of blood flow in human fetal left ventricles based on patient-specific 4D ultrasound scans. Biomech. Model. Mechanobiol.
Le, T.B., Sotiropoulos, F., 2012. On the three-dimensional vortical structure of early diastolic flow in a patient-specific left ventricle. Eur. J. Mech. B Fluids 35, 20–24.
Martínez-Legazpi, P., Bermejo, J., Benito, Y., Yotti, R., del Villar, C.P., González-Mansilla, A., Barrio, A., Villacorta, E., Sánchez, P.L., Fernández-Avilés, F., 2014. Contribution of the diastolic vortex ring to left ventricular filling. J. Am. Coll. Cardiol. 64, 1711–1721.
Mihalef, V., Ionasec, R.I., Sharma, P., Georgescu, B., Voigt, I., Suehling, M., Comaniciu, D., 2011. Patient-specific modelling of whole heart anatomy, dynamics and haemodynamics from four-dimensional cardiac CT images. Interface Focus 1, 286–296.
Osman, N.F., Prince, J.L., 2000. Visualizing myocardial function using HARP MRI. Phys. Med. Biol. 45, 1665–1682.
Pedrizzetti, G., Domenichini, F., 2005. Nature optimizes the swirling flow in the human left ventricle. Phys. Rev. Lett. 95, 108101.

Pedrizzetti, G., La Canna, G., Alfieri, O., Tonti, G., 2014. The vortex–an early predictor of cardiovascular outcome? Nat. Rev. Cardiol. 11, 545–553.
Rosentrater, K.A., Flores, R.A., 1997. Physical and rheological properties of slaughterhouse swine blood and blood components. Trans. Am. Soc. Agric. Eng., 40
Schenkel, T., Malve, M., Reik, M., Markl, M., Jung, B., Oertel, H., 2009. MRI-based CFD analysis of flow in a human left ventricle: methodology and application to a healthy heart. Ann Biomed Eng 37, 503–515.
Seo, J.H., Vedula, V., Abraham, T., Lardo, A.C., Dawoud, F., Luo, H., Mittal, R., 2014. Effect of the mitral valve on diastolic flow patterns. Phys. Fluids 26, 121901.
Vasudevan, V., Low, A.J.J., Annamalai, S.P., Sampath, S., Poh, K.K., Totman, T., Mazlan, M., Croft, G., Richards, A.M., de Kleijn, D.P.V., Chin, C.L., Yap, C.H., 2017. Flow dynamics and energy efficiency of flow in the left ventricle during myocardial infarction. Biomech. Model. Mechanobiol. 16, 1503–1517.
Vedula, V., Seo, J.-H., Lardo, A.C., Mittal, R., 2016. Effect of trabeculae and papillary muscles on the hemodynamics of the left ventricle. Theor. Comput. Fluid Dyn. 30, 3–21.
Watanabe, H., Sugano, T., Sugiura, S., Hisada, T., 2004. Finite element analysis of ventricular wall motion and intra-ventricular blood flow in heart with myocardial infarction. JSME Int. J. Ser. C Mech. Syst. Mach. Elem. Manuf. 47, 1019–1026.
Wiputra, H., Lim, G.L., Chia, D.A.K., Mattar, C.N.Z., Biswas, A., Yap, C.H., 2016. Methods for fluid dynamics simulations of human fetal cardiac chambers based on patient-specific 4D ultrasound scans. J. Biomech. Sci. Eng. 11, 1–13.
Wiputra, H., Lim, G.L., Chua, K.C., Nivetha, R., Soomar, S.M., Biwas, A., Mattar, C.N.Z., Leo, H.L., Yap, C.H., 2017. Peristaltic-like motion of the human fetal right ventricle and its effects on fluid dynamics and energy dynamics. Ann. Biomed. Eng., 1–13.